Research Article | Vol. 28, No. 13 / 22 June 2020 / Optics Express 19492

Optics EXPRESS

Manipulating the scattering pattern with non-Hermitian particle arrays

YUN JING ZHANG,[1,2] PENG LI,[1] VINCENZO GALDI,[3] MEI SONG TONG,[4] AND ANDREA ALÙ[2,5,6,*]

[1]School of Electronic and Information Engineering, Soochow University, Suzhou 215006, China
[2]Department of Electrical and Computer Engineering, The University of Texas at Austin, Austin 78712, USA
[3]Fields and Waves Lab, Department of Engineering, University of Sannio, I-82100 Benevento, Italy
[4]Department of Electronic Science and Technology, Tongji University, Shanghai 201804, China
[5]Photonics Initiative, Advanced Science Research Center, City University of New York, New York 10031, USA
[6]Physics Program, Graduate Center, City University of New York, New York 10016, USA
[*]aalu@gc.cuny.edu

Abstract: We show that an array of non-Hermitian particles can enable advanced manipulations of the scattering pattern, beyond what is possible with passive structures. Active linear elements are shown to provide zero forward scattering without sacrificing the total scattered power, and by adding more particles, it is possible to control the zero-scattering direction at will. We apply our theory to realistic implementations of scatterer arrays, using loaded dipole antennas in which we tune the load impedance and investigate the stability of these arrays based on a realistic dispersion model for the gain elements. Finally, we discuss the possibility of controlling multiple frequencies to enable broadband control of the scattering pattern.

1. Introduction

Scattering is the process by which objects extinguish a portion of energy from the incident wave and re-radiate it into the surrounding space. Controlling the scattering properties has been a topic of relevant interest for a long time in a multitude of applications, and it has inspired more recent research activities, including cloaking [1,2], nanoantennas [3,4], sensors [5,6], light-emitting devices [7] and photovoltaics [8]. The need for ultralow scattering cross sections has led to the development of metamaterial cloaking, also of interest for non-invasive near-field measurements [9,10]. Absorbing screens and antireflection coatings have been used for long time to suppress the scattering and reflections [11,12], but suitably designed metamaterial coatings can be used to lower the total scattering cross section, suppressing not only back reflections but also shadows (forward scattering), realizing nearly transparent objects [13]. However, the structural complexity and inherent limitations on bandwidth vs. electrical size of the objects that can be cloaked, stemming from causality, linearity and passivity considerations, impose severe restrictions on the applicability of these concepts [14,15]. If the direction of the impinging wave is known, unidirectional cloaks have been proposed, overcoming some of these trade-offs [16,17]. When illuminated from other directions, however, the scattering cross section of the cloaked object, becomes large in this case.

Passivity imposes other constraints on scattering. In particular, the optical theorem implies that zero forward-scattering can never be realized in passive systems [18], unless also the total scattering and absorption also go to zero. Nearly zero forward-scattering and larger scattering in other directions were predicted by Kerker, but they can be achieved only for weakly scattering magnetodielectric particles with small electrical size [18]. Zero scattering, including forward and backward scattering by bi-anisotropic particles, such as omega and chiral particles, has been

#395942 https://doi.org/10.1364/OE.395942
Journal © 2020 Received 24 Apr 2020; revised 4 Jun 2020; accepted 4 Jun 2020; published 17 Jun 2020

Optics EXPRESS

investigated in [19]. Reference [20] presented dimer- and triple-dipole antennas with unusual scattering patterns, including zero-forward scattering taking advantage of active systems.

In a different context, non-Hermitian systems, where gain and loss can be introduced in a controllable manner, have been recently explored in a variety of platforms, including in optics, acoustics and microwave engineering, showing peculiar responses such as power oscillations, absorption-enhanced transmission and unidirectional invisibility [21–24]. Of particular interest in this context are systems satisfying parity-time (PT-) symmetry, i.e., falling onto themselves after a parity and time-reversal operation [25]. In optics, these systems correspond to structures with balanced gain and loss [26]. Asymmetric scattering patterns in *PT*-symmetric particles have been recently investigated [27–29] and one-dimensional (1D) non-Hermitian structures that realize unidirectional invisibility have been proposed [30–32]. In 2D geometries, *PT*-symmetric coatings were designed to cloak a conducting cylinder [33,34]. Recently, balanced gain and loss dimers have been proposed to manipulate the radiation of a dipole emitter, which has important potential for nanoantennas [35].

In this work, using coupled-dipole theory, we explore the conditions to achieve zero scattering along arbitrary directions in non-Hermitian particle arrays. We verify our predictions in nanosphere and passive dipole antenna arrays. In Section II, we present the formalism for zero forward-scattering at different incidence angles for particle arrays. In Section III, we study the manipulation of the direction of zero-scattering by tuning the particle polarizabilities, overcoming the limitations of passive particles. In Section IV, we analyze the stability of these active systems, verifying that the proposed geometries can be made inherently stable. Next, in Section V, we explore the design of realistic dipole antenna configurations in the microwave frequency range, showing that the direction of zero scattering can be steered by modulating negative-resistance loads. Finally, in Section VI, we discuss the possibility of broadband implementations and provide an outlook.

2. Zero forward scattering in non-Hermitian arrays

Implementing zero scattering features using coupled dipole arrays has been explored in several papers, e.g., [36–39], offering possible implementations using nanocircuits or nanoantennas. Particularly challenging is the implementation of zero forward scattering with the incidence of transvers plane waves, because in this case the optical theorem relates the forward scattering and the total extinction cross section [40,41]

$$\sigma_{ext} = \frac{4\pi}{k} Im\{f(\theta = 0)\}, \tag{1}$$

where f is the scattered far-field (reduced) amplitude, θ is the observation angle, k is the wavenumber in background medium for the incident wave of which the direction is defined by $\theta = 0$.

The extinction cross section is the sum of the scattering and absorption cross sections, which for passive objects are both strictly non-negative quantities. Equation (1) indicates that, as long as scattering and absorption are non-zero, the forward scattering amplitude, or at least its imaginary part, cannot vanish. To achieve truly zero forward scattering in a passive particle, both absorption and scattering have to vanish, as in a cloaked particle.

If gain is introduced, however, the energy radiated by the active element as a response to the excitation acts as negative absorption, and therefore the extinction cross section becomes

$$\sigma_{ext} = \sigma_{abs} - \sigma_g + \sigma_{sca}, \tag{2}$$

where σ_{abs}, σ_g, σ_{sca} are the cross section of absorption, radiation and scattering, respectively. Even though all three quantities remain positive, now the total power extinguished from the impinging wave, i.e., the extinction cross section, and hence the forward scattering, can be made

Optics EXPRESS

zero through the introduction of sufficient gain [42]. Hence, in non-Hermitian systems, zero forward scattering can be achieved even for electrically large objects that scatter considerably. The requirement is that the total scattered power is not extracted from the impinging wave, but instead taken from the active elements in the system. In this paper, we explore these concepts specifically applied to dipole arrays, such as the n-dipole-array configuration shown in Fig. 1.

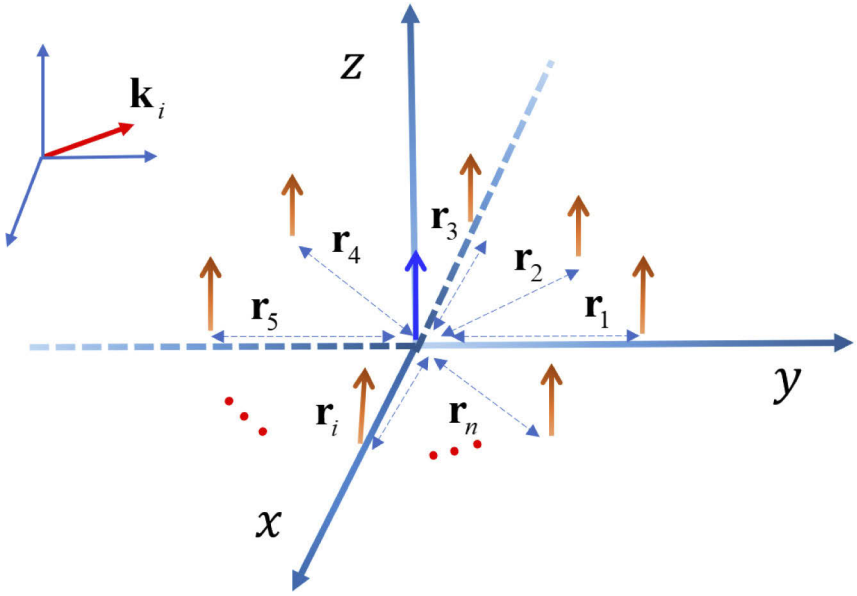

Fig. 1. $n-$ dipole array configuration.

A number of dipolar scatterers are located in the $x-y$ plane ($i = 1, 2 \ldots n$) at position $\boldsymbol{r}_i$. The incident electric field for each dipole is $\boldsymbol{E}_i(x, y, z) = \hat{x}E_{ix} + \hat{y}E_{iy} + \hat{z}E_{iz}$ and the corresponding induced dipole moment is

$$\mathbf{p}_i = \alpha_i \mathbf{E}_{ti}, \tag{3}$$

where $\mathbf{p}_i = \hat{x}p_{ix} + \hat{y}p_{iy} + \hat{z}p_{iz}$ and $\mathbf{E}_{ti}$ is the total electric field at the i-th dipole.

The total electric field at each dipole includes the incident field and the field induced by the other dipoles in the array, thus

$$\mathbf{E}_{ti} = \mathbf{E}_i + \sum\nolimits_{\substack{1\le j\le n \\ j\neq i}} \frac{k^2}{\varepsilon}\overline{\overline{G}}(\mathbf{r}_i - \mathbf{r}_j)\mathbf{p}_j, \tag{4}$$

where ε is the permittivity of the background, $\boldsymbol{r}_{i(j)}$ is the position vector of the $i(j)$-th dipole, and $\overline{\overline{G}}$ is the dyadic Green's function, which is given by

$$\overline{\overline{G}}(\mathbf{r}_i - \mathbf{r}_j) = (\bar{\bar{I}} + \frac{1}{k^2}\nabla\nabla)g(|\mathbf{r}_i - \mathbf{r}_j|), \tag{5}$$

where $\bar{\bar{I}}$ is the identity dyadic, $g(|\mathbf{r}_i - \mathbf{r}_j|) = e^{ik|\mathbf{r}_i - \mathbf{r}_j|}/4\pi|\mathbf{r}_i - \mathbf{r}_j|$, and an implicit $e^{-i\omega t}$ time-harmonic dependence is assumed.

We first investigate a canonical dimer system composed of two dipoles. We assume the dipole elements to be located along x, and polarized with angles φ_i with respect to the z axis. In this

Optics EXPRESS

scenario, from Eqs. (3)–(5) we find

$$\begin{pmatrix} 1 & -\alpha_1 A\cos^2\varphi_1 & 0 & -\alpha_1(A+B)\cos\varphi_1\sin\varphi_1 \\ 0 & -\alpha_1 A\cos\varphi_1\sin\varphi_1 & 1 & -\alpha_1(A+B)\sin^2\varphi_1 \\ -\alpha_2 A\cos^2\varphi_2 & 1 & -\alpha_2(A+B)\cos\varphi_2\sin\varphi_2 & 0 \\ -\alpha_2 A\cos\varphi_2\sin\varphi_2 & 0 & -\alpha_2(A+B)\sin^2\varphi_2 & 1 \end{pmatrix} \begin{pmatrix} p_{1z} \\ p_{2z} \\ p_{1x} \\ p_{2x} \end{pmatrix} \tag{6}$$

$$= \begin{pmatrix} \alpha_1\cos^2\varphi_1 E_{1z} + \alpha_1\cos\varphi_1\sin\varphi_1 E_{1x} \\ \alpha_1\cos\varphi_1\sin\varphi_1 E_{1z} + \alpha_1\sin^2\varphi_1 E_{1x} \\ \alpha_2\cos^2\varphi_2 E_{2z} + \alpha_2\cos\varphi_2\sin\varphi_2 E_{2x} \\ \alpha_2\cos\varphi_2\sin\varphi_2 E_{2z} + \alpha_2\sin^2\varphi_2 E_{2x} \end{pmatrix}$$

where $A = k^2(1+i/kd-1/k^2d^2)g(d)/\varepsilon$, $B = k^2(-1-3i/kd+3/k^2d^2)g(d)/\varepsilon$, and d is the distance between the two dipoles. If the dipole orientation is along the z-axis, and the impinging wave is z-polarized with wave vector parallel to the $x-y$ plane, Eq. (6) reduces to [43]

$$p_{iz} = \alpha_i \frac{E_{iz} + \alpha_j \mathrm{A} E_{jz}}{1 - \alpha_i\alpha_j A^2}\ , \tag{7}$$

where $(i,j) = (1,2)\ or\ (2,1)$.

The scattered electric far field can be written as

$$\mathbf{E}_{far} = \frac{k^2}{\varepsilon}\sum_i \overline{\overline{G}}(\mathbf{r}_{far} - \mathbf{r}_i)\mathbf{p}_i, \tag{8}$$

where $\mathbf{r}_{far}$ is the observation point in the far-field.

Zero forward scattering for an incident wave vector forming an angle η with respect to the x-axis, based on Eq. (8), is achieved when

$$\alpha_2 = -\frac{\alpha_1 e^{ikd\cos\eta}}{\alpha_1 A(e^{i2kd\cos\eta}+1) + e^{ikd\cos\eta}}. \tag{9}$$

In order to explore the physical implications of this condition, we first assume that the dimer is composed of two spherical particles of radius R, as shown in Fig. 2. When the electrical size is very small ($kR<<1$), the polarizability is given by $\alpha = (\alpha_0^{-1} - ik^3/6\pi\epsilon)^{-1}$, where $\alpha_0 = 4\pi R^3(\epsilon_r-1)/(\epsilon_r+2)$ is the quasi-static polarizability and ϵ_r is the relative permittivity of the spheres [1,2]. For metallic particles, the permittivity obeys the Drude model

$$\epsilon_r(\omega) = \epsilon_\infty - \frac{\omega_p^2}{\omega^2 + i\omega\gamma_p}, \tag{10}$$

where ϵ_∞ is the high-frequency limit, ω_p the plasma angular frequency, and γ_p a dampening term. Here, we set $\epsilon_\infty = 2$ and $\gamma_p = 0.05\omega_p$ to approximately model realistic conductive oxides at frequencies below their band gap [44].

Figure 3 shows the relative permittivity dispersion for a normalized frequency ranging from 0.5 to 1. It can be seen that, when $f/f_p<0.71$, the particle shows plasmonic properties. We assume that the left sphere in Fig. 2 is made of this conductive oxide material, and explore the required permittivity for the right sphere to yield zero forward scattering, assuming the dimensionless parameters $d/\lambda = 0.8$, $R/\lambda = 0.1$.

Figure 4 shows the relative permittivity of the second particle to realize zero forward scattering for a normalized frequency ranging from 0.5 to 1, and an arbitrary incident angle. Because the

Optics EXPRESS

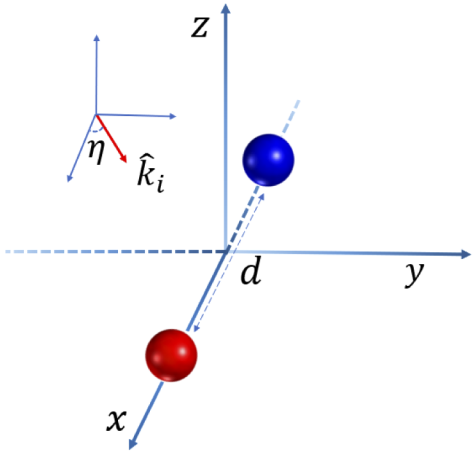

Fig. 2. Nanosphere dimer configuration.

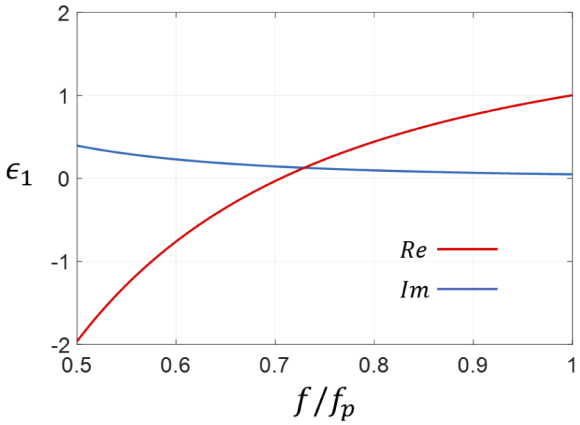

Fig. 3. Relative permittivity dispersion of lossy particles (conductive oxides). f/f_p is the operating frequency normalized with respect to the plasma frequency.

system is reciprocal, the forward scattering for opposite directions is identical [45], and therefore the required permittivity for incident angles between 180° to 360° is the same as for angles between 0° and 180°. In addition, $\epsilon_2(\eta) = \epsilon_2(\pi - \eta)$ because of symmetry, which is consistent with Eq. (9). Importantly, the imaginary part of the required permittivity for the second particle is negative, which implies that gain material is needed to realize zero forward scattering, consistent with Eq. (2). The polarizability of the sphere is a monotonic function of its permittivity for the case in Fig. 3; hence, we can derive the necessary but not sufficient condition for which the non-Hermitian particle has minimum or maximum gain level

$$\frac{\partial \alpha_2}{\partial \eta} = e^{i2kd\cos\eta} - 1 = 0. \tag{11}$$

The corresponding zero-scattering angle is

$$\eta = \arccos\frac{q\pi}{2kd},\ q = \pm 1,\ \pm 2\ldots. \tag{12}$$

Within a 90° range of the incident angle, the required gain can have two extrema at $\eta = 51.3°$ and 71.8°. The gain values at these two angles correspond to the maximum and minimum

Optics EXPRESS

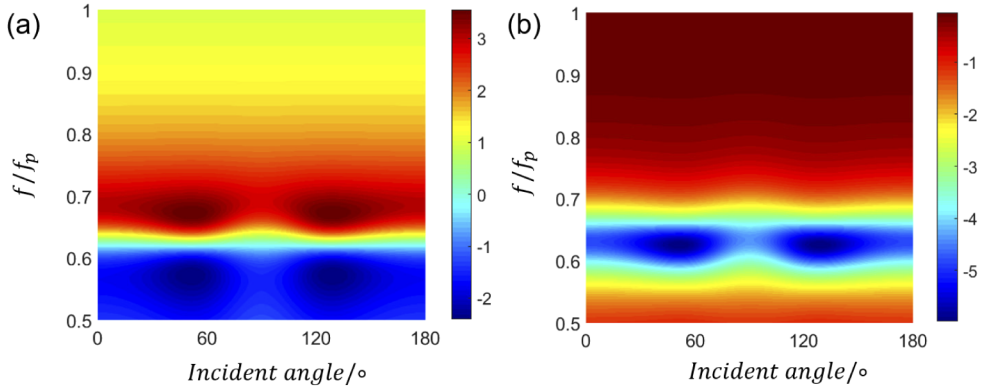

Fig. 4. Calculated relative permittivity ϵ_2 of the second sphere to achieve zero forward scattering, as a function of normalized frequency and incident angle. (a) Real part. (b) Imaginary part.

required level, as shown in Fig. 4. Notably, outside the plasmonic range (above $f/f_p \sim 0.7$), the required gain becomes lower and the real part of the relative permittivity asymptotically approaches unity, consistent with the permittivity dispersion of the passive particle, as shown in Fig. 3. In order to explore the radiation patterns in this regime, we choose $f/f_p = 0.8$, i.e., $\epsilon_1 = 0.4436 + 0.0973i$.

Figure 5 shows the normalized scattered electric field magnitude ($|r_{far}\mathbf{E}_{sca}|$) for dimers designed to support zero forward scattering for three incident angles 0, $\pi/4$ and $\pi/2$. Here $\lambda = 500\ nm$ and the incident electric field $E = 1\ V/m$. The corresponding permittivity ε_2 for the three gain particles are $1.8591 - 0.2439i$, $1.8125 - 0.2898i$, and $1.8024 - 0.3351i$. Here the horizontal plane is the $x-y$ plane as shown in Fig. 2, and the vertical plane is the plane containing the z axis and the incident direction $\mathbf{k}_i$. When the incident angle is $\pi/2$, the scattered electric field is almost zero in the $y-z$ plane, owing to the opposite scattering phase from the two particles, hence, the radiation in the plane is not plotted. It can be seen that the analytical predictions

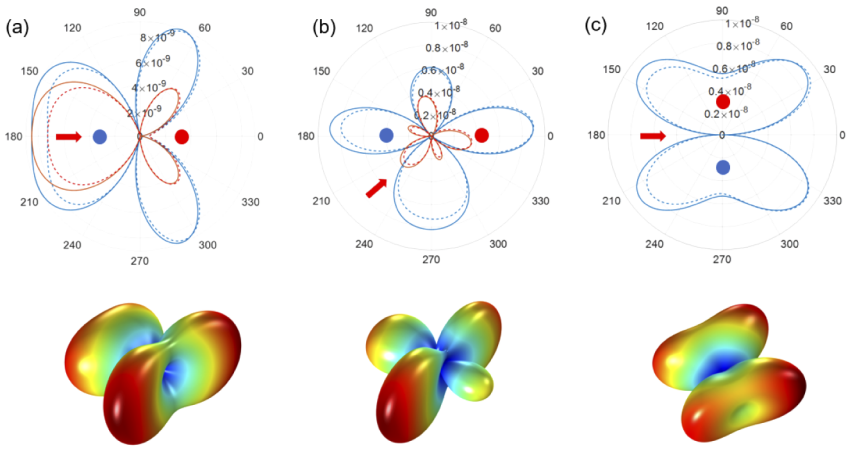

Fig. 5. Scattering patterns with incident angles (a) 0 (b) $\pi/4$ and (c) $\pi/2$ and dimers optimized to support zero forward scattering. Blue solid and dashed lines pertain to the analytical and numerical scattering patterns, respectively, in the horizontal plane. Red solid and dashed lines pertain to the vertical plane. The scattered field value is scaled to $|r_{far}\mathbf{E}_{sca}|$.

Optics EXPRESS

and the numerically computed results, obtained via finite-element simulations, show a good agreement. The difference between simulated and analytical results is attributed to the influence of higher-order multipole harmonics from the spherical particles, which are neglected in our simplified analytical model. For different incident angles, the scattering pattern is rather different, yet always ensuring zero forward scattering, hence zero extinction from the impinging wave and no shadows. The scattered energy, in other words, is solely due to the radiation from the dimer as a reaction to the excitation, while the impinging wave is not affected by the interaction with the dimer.

3. Manipulating the direction of zero scattering

Given that it is possible to induce zero forward scattering with a non-Hermitian dimer, it is of interest to explore if a proper design of the dimer may route the scattering towards other directions. This may be of interest for nanoantenna tunability and reconfigurability [46,47].

In order to study this problem more generally, we consider, as shown in Fig. 6, the entire solid angle sphere around the dimer, with azimuthal angle η and elevation angle γ. In order to achieve a scattering zero at the azimuthal angle φ and elevation angle θ, we need

$$\alpha_2 = -\frac{\alpha_1 e^{ikd\cos\varphi\sin\theta}}{\alpha_1 A[e^{ikd(\cos\varphi\sin\theta+\cos\eta\sin\gamma)}+1]+e^{ikd\cos\eta\sin\gamma}}. \tag{13}$$

In order to study the phenomenon, we consider an incident wave with $\gamma = \pi/2$ and $\eta = 0$, and study the conditions on the dimer to achieve arbitrary direction for the zero scattering condition. In particular, we focus on small separation d ($d/\lambda = 0.8$), for which the role of the dimer is crucial and the scattering zero has a relatively large angular beamwidth.

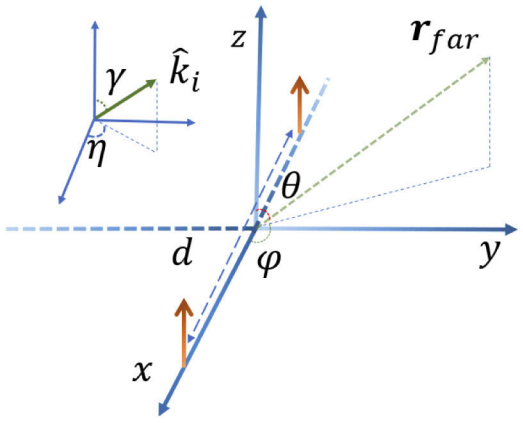

Fig. 6. Coordinate system to analyze the radiation pattern of a dimer.

Figures 7(a) and 7(b) plot the required relative permittivity of the second particle to yield zero scattering in the direction of choice, as a function of its azimuth and elevation angles. The permittivity is symmetric along the lines $\theta = \pi/2$ and $\varphi = \pi$, as expected because of symmetry and reciprocity. Figure 7(b) shows that, besides forward scattering, realizing zero-scattering in other directions may also require gain. Therefore, through permittivity modulation of the second particle, the first particle can be hidden along arbitrary designated directions. For this dimer, nearly zero forward scattering is achieved for different values of distance between the two particles (see Appendix 1). This can be explained by the fact that in the forward direction, according to Eqs. (7) and (8), the dipole moments of the two particles with different distance both

Optics EXPRESS

show a phase delay or phase advance consistent with the original distance, hence, still satisfying zero forward scattering.

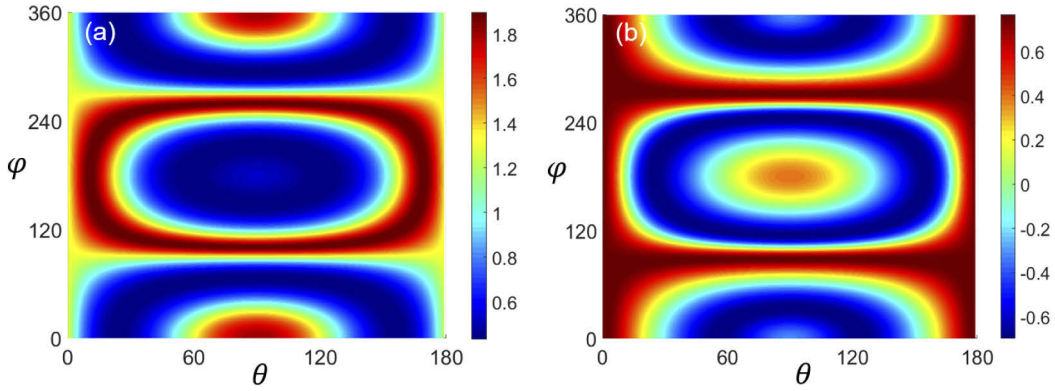

Fig. 7. Relative permittivity ϵ_2 of the second particle to implement zero scattering in the desired direction. (a) real part; (b) imaginary part.

The scattering patterns, normalized to the scattered electric far field peak, with different directions of zero scattering are plotted in Fig. 8. In order to display the patterns clearly, we consider $d/\lambda = 1/3$ ($\lambda = 500\ nm, f/f_p = 0.8$) which ensures a pattern with limited number of beams. The calculated permittivity for the second nanosphere is given in Table 1, with reference to a companion lossy nanosphere with relative permittivity $\epsilon_1 = 0.4436 + 0.0973i$. It can be seen that the modulation of permittivity for the second particle also leads to the reconfiguration of the scattering pattern.

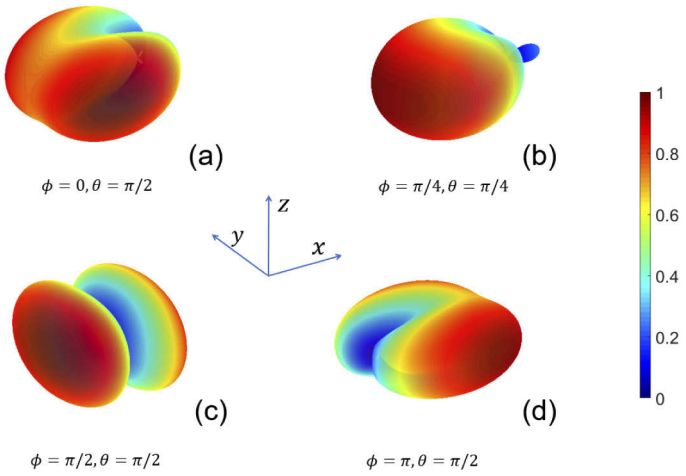

Fig. 8. Scattering patterns of the dimer for different directions of zero scattering (the incident direction is at $\eta = 0$ and $\gamma = \pi/2$).

Equation (11) suggests that, when the permittivity of the first particle is known, only one direction can be set to zero scattering through modulation of the second particle. Multiple directions of zero scattering for the particle array may be achieved by adding more particles, as shown in Fig. 1. According to Eqs. (3) and (4), if there are n dipoles in the system with a specified incident wave, n equations can be established. We assume the polarizability of one lossy particle to be manipulated in terms of its scattering is assigned; then, n unknown $\mathbf{p}_i$ and $n-1$ unknown

Optics EXPRESS

Table 1. Calculated relative permittivity of the second sphere for different directions of zero scattering in Fig. 8.

	(a)	(b)	(c)	(d)
ϵ_2	1.8736-0.2689i	1.7989-0.2869i	1.7888-0.2637i	1.8168-0.3375i

α_i are to be determined. From Eq. (8), we know that one direction of zero scattering corresponds to one additional equation. To maintain consistency, no more than $n-1$ equations can be added. Therefore, if the system is full-ranked, i.e., it has exactly one solution, $n-1$ directions of zero scattering can be realized and controlled. As an illustration, a four-sphere array is considered, as shown in Fig. 9. For easy implementation we assume the radii to be all equal, $R = \lambda/10$ ($\lambda = 500\ nm$), and the distance between particles and origin $r = \lambda/2$. We stress, however, that the analysis can be applied to any multi-nanosphere system with different R and r.

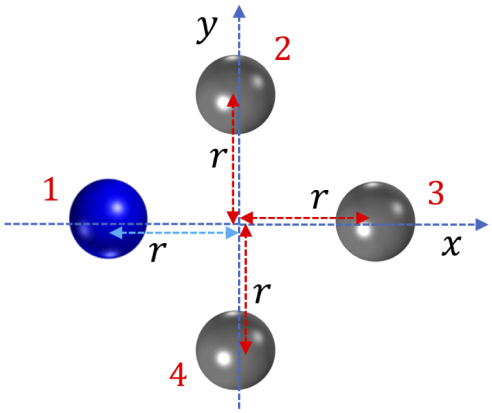

Fig. 9. Four-nanosphere system.

In this system, three directions of zero scattering can be realized, i.e.,

$$\sum_{i=1}^{3}\sum_{j=1}^{3}\mathbf{E}_{sca}^{i}(\theta_i,\varphi_i)\delta_{ij}=0. \tag{14}$$

The permittivity of the blue nanosphere (left particle) in this system is assumed to follow Eq. (10). Then, the permittivity of the other spheres can be determined depending on the desired direction of zero scattering and the incident wave.

We assume that the incident wave is z-polarized and the wave vector is along the x-direction. Two cases are chosen, one for which the zero-scattering conditions are enforced at the directions $(\theta, \varphi) = \{(\pi/2, 0), (\pi/2, \pi/2), (\pi/2, \pi)\}$ is zero, and the other at directions $\{(\pi/4, 0), (\pi/2, \pi/2), (\pi/4, \pi)\}$. Using Eqs. (4) and (8), the permittivity of the other three spheres can be calculated as in Table 2. It can be seen that gain material may be required, depending on the required directions of zero scattering. Figure 10 plots the normalized scattered electric far field pattern in the two scenarios, respectively. Simulated and calculated results show a good agreement, with the slight difference again attributed to the higher-order multipole moments of the nanospheres.

It is worth mentioning that, instead of modulating the permittivity of the spheres to realize multi-direction of zero scattering, the distance can be tuned as well.

Optics EXPRESS

Table 2. Calculated relative permittivity of nanospheres.

	ϵ_1	ϵ_2	ϵ_3	ϵ_4
Case I	0.4436+0.0973i	1.8603-0.2811i	0.8564-0.6601i	0.7760+0.6768i
Case II	0.4436+0.0973i	1.3948-0.9003i	0.8744-0.6482i	0.3931+0.4436i

4. Stability analysis

The scattering patterns presented above assume that the system is in steady state with a monochromatic incident wave. However, a realistic causal excitation requires stability to be satisfied for all frequencies, which is not guaranteed in a system with gain. The dispersion of the gain material can be represented by adding a two-level gain profile to Eq. (10), which is written as [26]

$$\varepsilon_G(\omega) = \varepsilon_L(\omega) + K\frac{\gamma_0}{\omega - \omega_0 + i\gamma_0}, \tag{15}$$

where the coefficient K is controlled by the pumping level, γ_0 is the gain bandwidth coefficient, and ω_0 is the resonant angular frequency.

From Eqs. (3), (4), and (8), the scattered electric far field is determined by the superposition of the radiation from all dipoles

$$\mathbf{E}_{far} = \frac{k^2}{\varepsilon}\sum_{i=1}^{n}\overline{\overline{G}}(\mathbf{r}_{far} - \mathbf{r}_i)\mathbf{p}_i\{\alpha_1, \alpha_2, \ldots, \alpha_n; \mathbf{r}_1, \mathbf{r}_2, \ldots, \mathbf{r}_n; \mathbf{E}_i\}. \tag{16}$$

Modeling the system as in system theory, the transfer function reads

$$H(\omega) = \frac{|\mathbf{E}_{far}|}{|\mathbf{E}_i|}. \tag{17}$$

The poles of this function need to be in the lower half of the complex frequency plane ($Im\{\omega\}<0$) to ensure stability. We start by assuming a realistic model for $\varepsilon_L(\omega)$, following Eq. (10), with a pumping level K set to 0.55. We set the normalized angular frequency $\omega/\omega_p = N_1$ (ω_p is the plasmonic angular frequency of lossy term) and for the gain term $\gamma_0 = \gamma\omega_0$. Then Eqs. (10) and (15) can be expressed as

$$\begin{cases} \varepsilon_L(\omega) = \varepsilon_\infty - \frac{1}{N_1^2 + i0.05N_1} \\ \varepsilon_G(\omega) = \varepsilon_L(\omega) + \frac{0.55\gamma}{N_1\omega_p/\omega_0 + i\gamma - 1} \end{cases}. \tag{18}$$

Here we assume the lossy term of gain nanosphere is the same with the dispersive permittivity of loss nanosphere [Eq. (10)] except ε_∞. Hence, if the ratio γ is given, ω_0 and ε_∞ of the gain nanosphere can be determined uniquely to satisfy the needed permittivity of the gain nanosphere. Then Eq. (17) can be plotted with varying frequencies. Figure 11 shows the pole distributions for the three cases illustrated in Fig. 5. The operating frequency is normalized with respect to the plasma frequency, i.e., N_1. Here the value of $H(N_1)$ is expressed in negative logarithmic scale.

It can be seen that all poles are in the lower half-plane, indicating that the system is stable for this choice of dispersion model. Near the real frequency axis, two poles are found at low frequencies, which correspond to the Fröhlich condition in the plasmonic range $Re\{\varepsilon_r\} = -2$. Near the operating frequency $\omega/\omega_p = 0.8$, the poles are far from the real axis, indicating good stability within the gain band.

For the four-sphere system, in addition to the known lossy nanosphere, we have other three lossy or gain nanospheres to be modeled in terms of the dispersive permittivity as in Fig. 9. We assume the lossy term to be the same as the known lossy nanosphere, except for the value of ε_∞. With reference to Table 2, the required ε_∞ and ω_0 can be calculated in the same way.

Optics EXPRESS

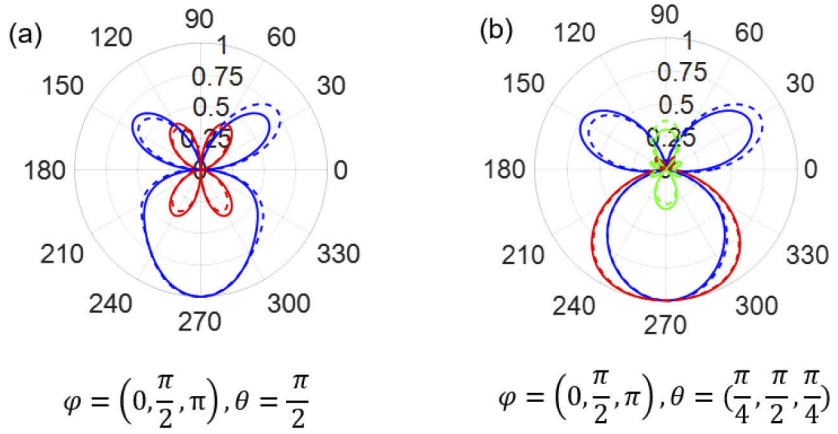

Fig. 10. Normalized scattering patterns of the four-sphere array (dashed and solid lines are analytical and simulated results, respectively. Blue, red and green line represent $x-y$, $x-z$ and $y-z$ planes, respectively). (a) Case I. (b) Case II.

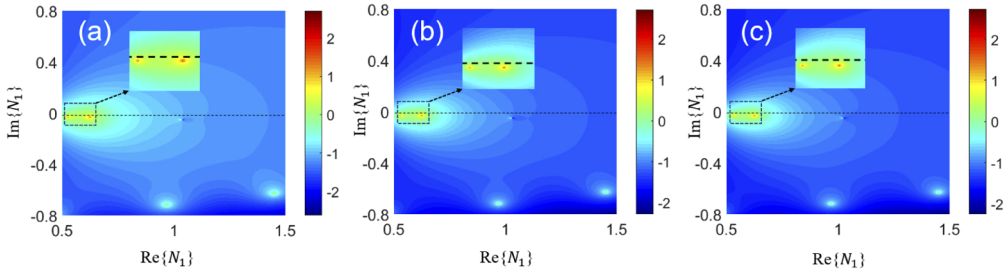

Fig. 11. Pole distributions of the transfer function $H(N_1)$ for three cases in Fig. 5 ($\gamma = 0.05$). (a) $N_2 = 0.9609$. (b) $N_2 = 0.9676$. (c) $N_2 = 0.9739$.

Then, the pole distributions for the two examples considered in Fig. 10 are plotted in Fig. 12. Similarly, besides the Fröhlich points, all poles are far below the real frequency axis, indicating that also the four-sphere system exhibits good stability. These results show that it is possible to realize arbitrary zero-scattering conditions in a stable manner in non-Hermitian arrays. Since we

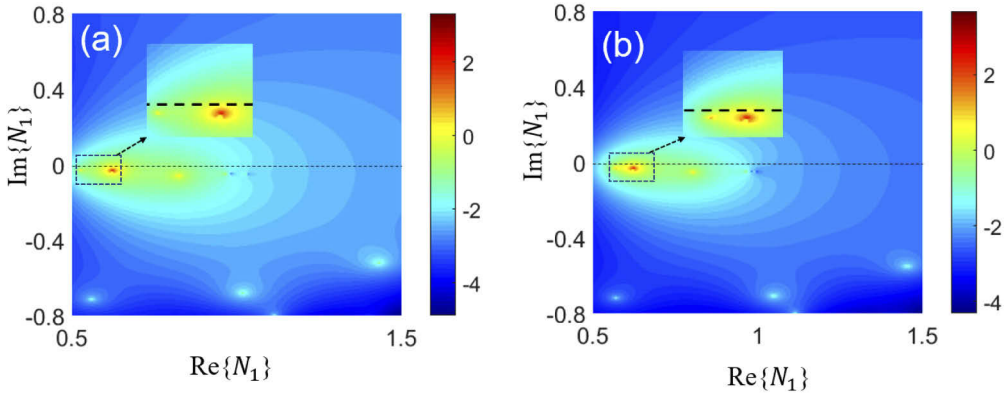

Fig. 12. Pole distributions for two cases in Fig. 10.

Optics EXPRESS

are not interested in lasing or highly resonant features, but instead in scattering suppression by combining gain and loss in the array, we do not experience particular challenges in designing stable systems, as long as we suitably tailor the gain dispersion over a narrow bandwidth around the frequency of interest.

5. Dipole antenna arrays

In order to explore a realistic implementation of the presented concepts, we investigate the case of electric dipole antenna arrays to manipulate the scattering pattern in non-Hermitian systems. From Ref. [48], the polarizability of short dipole antennas loaded by lumped elements is given by

$$\alpha = (-\frac{3\omega X_{in}}{l^2}\frac{X_{in}+iZ_L}{4X_{in}+iZ_L} - i\frac{k_0^3}{6\pi\varepsilon_0})^{-1}, \tag{19}$$

where X_{in} is the antenna reactance, Z_L is the load impedance, and l is the length of the antenna.

A dipole antenna dimer system is first investigated to achieve zero forward scattering. We assume the frequency of the incident wave to be 1 GHz, and the antennas to have equal length $\lambda/10$. The load impedance of the lossy dipole antenna is set to $(50 - i\ 200)\ \omega$ and the distance between the two antennas is λ. Using Eq. (11) for the longitudinal incident wave, we calculate the required load impedance for the other antenna to be $Z_g = (-12 - i\ 860)\ \omega$. This means that the antenna has gain and an inductive response, which can balance the resistance and capacitance of the lossy antenna. Figure 13 shows the scattered electric far-field (dB) of the dimer antenna, when a z-polarized wave impinges along the x-direction. It is observed that the forward scattering is 45 dB smaller than the peak value.

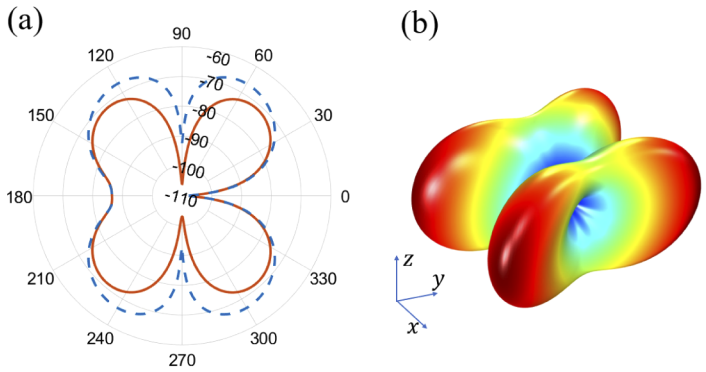

Fig. 13. Simulated scattering patterns of the dipole antenna dimer system: (a) Blue line: horizontal plane; red line: vertical plane. (b) 3D radiation pattern.

As another example, we require the scattering along $\varphi = \pi/3, \theta = \pi/2$ to be zero, then Eq. (11) yields a load impedance $(80 - i\ 200)\ \omega$. We can see that in this scenario, the load resistance is not necessarily negative. The scattering pattern is shown in Fig. 14. In contrast to the zero forward scattering case, we see that the direction along $4\pi/3$ also shows suppressed scattering because of symmetry: $\alpha_2(\varphi, \theta = \gamma = \pi/2,\ \eta = 0) = \alpha_2(2\pi - \varphi, \theta = \gamma = \pi/2,\ \eta = 0)$.

The stability analysis for dipole antenna arrays is similar to the one developed in the previous section: the gain component for electric circuits, i.e., negative resistance, obeys the relation $Z_g = -R_g(-\omega^2 + \omega_0^2 - i\ \gamma_e\omega_0\omega)/(-\omega^2 + \omega_0^2 + i\ \gamma_e\omega_0\omega)$ satisfying Kramers-Kronig relations, where R_g is the required negative resistance, γ_e is the bandwidth of the negative resistance, and ω_0 is the resonant angular frequency. In order to realize Z_g at 1 GHz, we may use an external inductor or capacitor tuning the bandwidth of the negative resistance to stabilize the system.

Optics EXPRESS

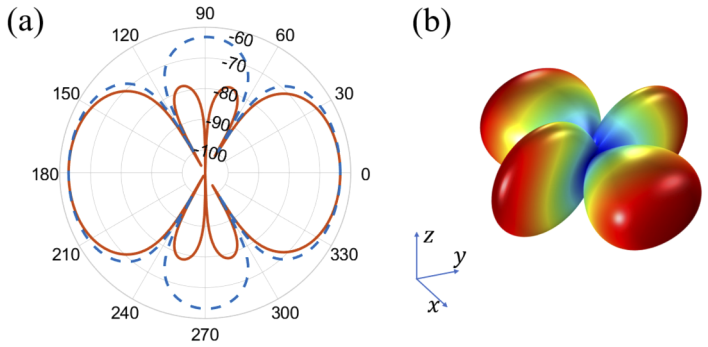

Fig. 14. Scattering patterns of the dipole antenna dimer system with the incident wave $\varphi = \pi/3, \theta = \pi/2$. (a) Blue line: horizontal plane; red line: vertical plane. (b) 3D radiation pattern.

6. Discussions and conclusions

In this paper, we have considered non-Hermitian arrays of scatterers to realize zero forward scattering and directional zero scattering in arbitrary directions, beyond the limitations implied by power conservation in passive systems. We have implemented these concepts in a nanosphere array, and in a dipole antenna array at microwave frequencies, in which, manipulating the lumped elements loading the antennas it is possible to control the directions of zero scattering from the array. We have also analyzed the stability of the system, and have shown that it is possible to attain unconditional stability.

The presented analysis has been limited to a single frequency; hence, the manipulation of zero scattering is expected to be narrow bandwidth. It is noted that when the particle array has n particles, $n-1$ directions of zero scattering can be simultaneously controlled. Sacrificing some directions of zero scattering, we may be able to realize zero scattering at multiple frequencies. As an example, if the forward scattering of a three-particle array is zero at two frequencies, the relations $\alpha_3(f_1) = F_1\{\alpha_2(f_1), \alpha_1(f_1)\}$ and $\alpha_3(f_2) = F_2\{\alpha_2(f_2),\ \alpha_1(f_2)\}$ should hold (F_1 and F_2 represents the generic function). Thanks to the dispersion in Eq. (15), we can tune the parameters of the other two particles to satisfy these two relations. Theoretically, we may be able to realize zero forward scattering over a finite frequency range using many-particle arrays, however the issue of stability is expected to inherently limit the overall bandwidth.

We believe that these results may be implemented at microwave frequencies using antenna arrays and at optical frequencies using nanoparticles, offering new opportunities to control and redirect the scattering from arrays of small scatterers.

Appendix 1

When the distance between two particles is changed from d to d_1, and the incident wave is with the azimuthal angle η_0 and elevation angle γ_0; then from Eqs. (7), (8), and (13), the forward scattered electric field is

$$E(d_1)|_{\gamma=\gamma_0}^{\eta=\eta_0} = \frac{k^2}{\varepsilon}\frac{e^{ik(r-d_1/2)}}{4\pi r}(p_1 e^{ikd_1\cos\eta\sin\gamma} + p_2) = \frac{k^2}{\varepsilon}\frac{e^{ikr}}{4\pi r}\frac{e^{ikd_1\cos\eta\sin\gamma}(\alpha_1+\alpha_2)+\alpha_1\alpha_2 A_{d1}(e^{ikd_1\cos\eta\sin\gamma}+1)}{1-\alpha_1\alpha_2 A_{d1}^2}, \tag{20}$$

where r is the distance between the observation point and the origin. The polarizabilities, α_1 and α_2, are not changed with the distance and still satisfy Eq. (13). For nanospheres, the second term in the numerator in Eq. (20) is $\sim r^2$ order of magnitude smaller than the first term, and hence it can be ignored. It indicates that the forward scattered electric field just exhibits a phase shift, but

Optics EXPRESS

not a variation of magnitude. We set the ratio c of the forward scattered electric field pertaining to distances d_1 and d as

$$c = \lim_{\substack{\eta\to\eta_0 \\ \gamma\to\gamma_0}} \left| \log \frac{E(d_1)}{E(d)} \right|. \tag{21}$$

If c is close to zero, then $E(d_1)$ has the same order of $E(d)$, and hence the forward scattering pertaining to the distance d_1 is almost zero. Figure 15 shows that compared with the original distance d between two nanospheres, the forward scattered electric field is almost zero with the distance between two nanospheres changed from 0.1λ to 1.2λ ($c \sim 0$).

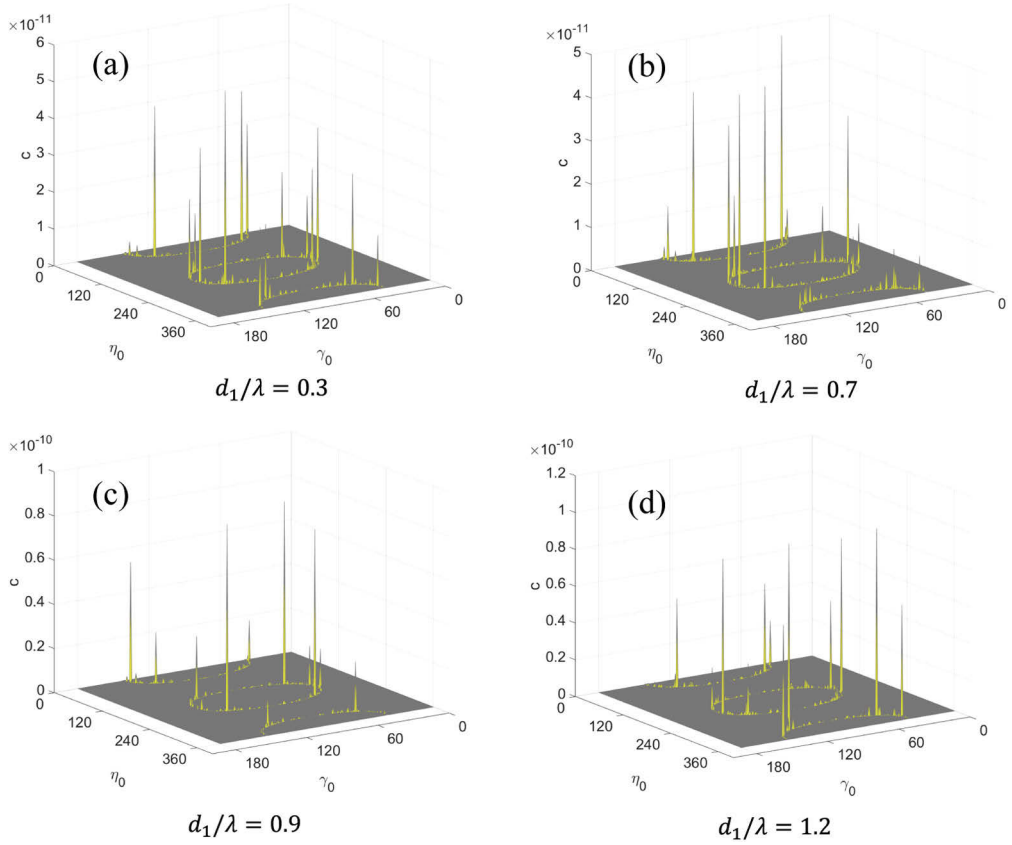

Fig. 15. Ratio c in Eq. (21) with different distances between two particles ($d = 200\ nm$, $\lambda = 500\ nm$, the two nanospheres have radii $r_1 = r_2 = 50\ nm$).

Funding

Air Force Office of Scientific Research; Simons Foundation; National Science Foundation.

Disclosures

The authors declare no conflicts of interest.

References

1. P. Y. Chen, J. Soric, and A. Alù, "Invisibility and cloaking based on scattering cancellation," Adv. Mater. **24**(44), OP281–OP304 (2012).

Optics EXPRESS

2. A. Alù and N. Engheta, "Achieving transparency with plasmonic and metamaterial coatings," Phys. Rev. E **72**(1), 016623 (2005).
3. L. Novotny and N. Van Hulst, "Antennas for light," Nat. Photonics **5**(2), 83–90 (2011).
4. A. G. Curto, G. Volpe, T. H. Taminiau, M. P. Kreuzer, R. Quidant, and N. F. V. Hulst, "Unidirectional emission of a quantum dot coupled to a nanoantenna," Science **329**(5994), 930–933 (2010).
5. A. V. Kabashin, P. Evans, S. Pastkovsky, W. Hendren, G. A. Wurtz, R. Pollard, V. A. Podolskiy, and A. V. Zayats, "Plasmonic nanorod metamaterials for biosensing," Nat. Mater. **8**(11), 867–871 (2009).
6. B. García-Cámara, R. Gómez-Medina, J. J. Sáenz, and B. Sepúlveda, "Sensing with magnetic dipolar resonances in semiconductor nanospheres," Opt. Express **21**(20), 23007–23020 (2013).
7. S. R. K. Rodriguez, F. B. Arango, T. P. Steinbusch, M. A. Verschuuren, A. F. Koenderink, and J. Gómez Rivas, "Breaking the symmetry of forward-backward light emission with localized and collective magnetoelectric resonances in arrays of pyramid-shaped aluminum nanoparticles," Phys. Rev. Lett. **113**(24), 247401 (2014).
8. C. Van Lare, F. Lenzmann, M. A. Verschuuren, and A. Polman, "Dielectric scattering patterns for efficient light trapping in thin-film solar cells," Nano Lett. **15**(8), 4846–4852 (2015).
9. A. Alù and N. Engheta, "Cloaked near-field scanning optical microscope tip for noninvasive near-field imaging," Phys. Rev. Lett. **105**(26), 263906 (2010).
10. J. C. Soric, P. Y. Chen, A. Kerkhoff, D. Rainwater, K. Melin, and A. Alù, "Demonstration of an ultralow profile cloak for scattering suppression of a finite-length rod in free space," New J. Phys. **15**(3), 033037 (2013).
11. R. L. Fante and M. T. McCormack, "Reflection properties of the Salisbury screen," IEEE Trans. Antennas Propag. **36**(10), 1443–1454 (1988).
12. J. Ward, "Towards invisible glass," Vacuum **22**(9), 369–375 (1972).
13. P. Alitalo and S. Tretyakov, "Electromagnetic cloaking with metamaterials," Mater. Today **12**(3), 22–29 (2009).
14. F. Monticone and A. Alù, "Do Cloaked Objects Really Scatter Less?" Phys. Rev. X **3**(4), 041005 (2013).
15. H. Hashemi, C.-W. Qiu, A. P. McCauley, J. D. Joannopoulos, and S. G. Johnson, "Diameter-bandwidth product limitation of isolated-object cloaking," Phys. Rev. A **86**(1), 013804 (2012).
16. B. Zhang, Y. Luo, X. Liu, and G. Barbastathis, "Macroscopic invisibility cloak for visible light," Phys. Rev. Lett. **106**(3), 033901 (2011).
17. M. Selvanayagam and G. V. Eleftheriades, "Experimental demonstration of active electromagnetic cloaking," Phys. Rev. X **3**, 041011 (2013).
18. A. Alù and N. Engheta, "How does zero forward-scattering in magnetodielectric nanoparticles comply with the optical theorem?" J. Nanophotonics **4**(1), 041590 (2010).
19. J. Vehmas, Y. Ra'di, A. O. Karilainen, and S. A. Tretyakov, "Eliminating electromagnetic scattering from small particles," IEEE Trans. Antennas Propag. **61**(7), 3747–3756 (2013).
20. M. Safari, M. Albooyeh, C. R. Simovski, and S. A. Tretyakov, "Shadow-free multimers as extreme-performance meta-atoms," Phys. Rev. B **97**(8), 085412 (2018).
21. G. Barontini, R. Labouvie, F. Stubenrauch, A. Vogler, V. Guarrera, and H. Ott, "Controlling the dynamics of an open many-body quantum system with localized dissipation," Phys. Rev. Lett. **110**(3), 035302 (2013).
22. P.-Y. Chen, M. Sakhdari, M. Hajizadegan, Q. Cui, M. M.-C. Cheng, R. El-Ganainy, and A. Alù, "Generalized parity-time symmetry condition for enhanced sensor telemetry," Nat. Electron. **1**(4), 297–304 (2018).
23. C. M. Bender and S. Böttcher, "Real spectra in non-Hermitian Hamiltonians having PT symmetry," Phys. Rev. Lett. **80**(24), 5243–5246 (1998).
24. S. Longhi, "PT-symmetry laser absorber," Phys. Rev. A **82**(3), 031801 (2010).
25. H. Hodaei, M. -Ali Miri, M. Heinrich, D. N. Christodoulides, and M. Khajavikhan, "Parity-time-symmetric microring lasers," Science **346**(6212), 975–978 (2014).
26. K. G. Makris, R. El-Ganainy, and D. N. Christodoulides, "Beam dynamics in PT symmetric optical lattices," Phys. Rev. Lett. **100**(10), 103904 (2008).
27. A. Manjavacas, "Anisotropic optical response of nanostructures with balanced gain and loss," ACS Photonics **3**(7), 1301–1307 (2016).
28. M. A. Miri, M. A. Eftekhar, M. Facao, A. F. Abouraddy, A. Bakry, M. A. N. Razvi, A. Alshahrie, A. Alù, and D. N. Christodoulides, "Scattering properties of PT-symmetric objects," J. Opt. **18**(7), 075104 (2016).
29. X. Chen, W. Yue, R. Tao, P. Yao, and W. Liu, "Scattering phenomenon of PT-symmetric dielectric-nanosphere structure," Phys. Rev. A **94**(5), 053829 (2016).
30. Z. Lin, H. Ramezani, T. Eichelkraut, T. Kottos, H. Cao, and D. N. Christodoulides, "Unidirectional invisibility induced by PT-Symmetry Periodic Structures," Phys. Rev. Lett. **106**(21), 213901 (2011).
31. L. Feng, Y. L. Xu, W. S. Fegadolli, M. H. Lu, J. E. Oliveira, V. R. Almeida, Y. F. Chen, and A. Scherer, "Experimental demonstration of a unidirectional reflectionless parity-time metamaterial at optical frequencies," Nat. Mater. **12**(2), 108–113 (2013).
32. R. Fleury, D. L. Sounas, and A. Alù, "An invisible acoustic sensor based on parity-time symmetry," Nat. Commun. **6**(1), 5905 (2015).
33. D. L. Sounas, R. Fleury, and A. Alù, "Unidirectional cloaking based on metasurfaces with balanced loss and gain," Phys. Rev. Appl. **4**(1), 014005 (2015).
34. A. Kord, D. L. Sounas, and A. Alù, "Active microwave cloaking using parity-time-symmetric satellites," Phys. Rev. Appl. **10**(5), 054040 (2018).

Optics EXPRESS

35. S. Sanders and A. Manjavacas, "Nanoantennas with balanced gain and loss," Nanophotonics **9**(2), 473–480 (2020).
36. T. Shibanuma, P. Albella, and S. A. Maier, "Unidirectional light scattering with high efficiency at optical frequencies based on low-loss dielectric nanoantennas," Nanoscale **8**(29), 14184–14192 (2016).
37. P. Albella, T. Shibanuma, and S. A. Maier, "Switchable directional scattering of electromagnetic radiation with subwavelength asymmetric silicon dimers," Sci. Rep. **5**(1), 18322 (2016).
38. L. Ge, L. Liu, S. Dai, J. Chai, Q. Song, H. Xiang, and D. Han, "Unidirectional scattering induced by the toroidal dipolar excitation in the system of plasmonic nanoparticles," Opt. Express **25**(10), 10853–10862 (2017).
39. B. G. Cámara, J. F. Algorri, A. Cuadrado, V. Urruchi, J. M. Sánchez-Pena, R. Serna, and R. Vergaz, "All-Optical Nanometric Switch Based on the Directional Scattering of Semiconductor Nanoparticles," J. Phys. Chem. C **119**(33), 19558–19564 (2015).
40. A. V. Krasavin, P. Segovia, R. Dubrovka, N. Olivier, G. A. Wurtz, P. Ginzburg, and A. V. Zayats, "Generalization of the optical theorem: experimental proof for radially polarized beams," Light: Sci. Appl. **7**(1), 36 (2018).
41. J. D. Jackson, *Classical Electrodynamics* (Wiley, 1999).
42. S. Tretyakov, "Maximizing Absorption and Scattering by Dipole Particles," Plasmonics **9**(4), 935–944 (2014).
43. A. A. Kuntman, E. Kuntman, J. S-Parramon, and O. Arteaga, "Light scattering by coupled oriented dipoles: Decomposition of the scattering matrix," Phys. Rev. B **98**(4), 045410 (2018).
44. J. Kin, G. V. Naik, N. K. Emani, U. Guler, and A. Boltasseva, "Plasmonic resonances in nanostructured transparent conducting oxide films," IEEE J. Sel. Top. Quantum Electron. **19**(3), 4601907 (2013).
45. D. L. Sounas and A. Alù, "Extinction symmetry for reciprocal objects and its implications on cloaking and scattering manipulation," Opt. Lett. **39**(13), 4053 (2014).
46. A. Alù and N. Engheta, "Tuning the scattering response of optical nanoantennas with nanocircuit loads," Nat. Photonics **2**(5), 307–310 (2008).
47. Y. H. Fu, A. I. Kuznetsov, A. E. Miroshnichenko, Y. F. Yu, and B. Lukyanchuk, "Directional visible light scattering by silicon nanoparticles," Nat. Commun. **4**(1), 1527 (2013).
48. A. Alù and S. Maslovski, "Power relations and a consistent analytical model for receiving wire antennas," IEEE Trans. Antennas Propag. **58**(5), 1436–1448 (2010).